Effect of Bearing Thermally Induced Preload on the Efficiency of Automotive Manual Transmission under RDE Driving Cycle

A. Laderou[1], M. Mohammadpour[1], S. Theodossiades[1], A. Wilson[2], R. Daubney[2]

[1] Wolfson School of Mechanical, Electrical and Manufacturing Engineering, Loughborough University, Loughborough, UK

[2] Ford Engineering Research Centre, Dunton, Laindon, Essex, UK

Abstract

In order to calculate the efficiency of an automotive manual transmission, taking into consideration the effect of its most power consuming components - gears and bearings - as well as the interactions between them, is of high importance. In this paper, a dynamic model has been developed which can predict the frictional losses of a complete gearbox as a system and, thus, its efficiency. The effect of temperature on bearing preload is also considered and taken into account from a system perspective identifying its effect on the bearings frictional losses (as well as the overall efficiency). The operating conditions used are snapshots of the RDE (Real Driving Emissions) driving cycle, which is a standard metric for automotive manufactures. Results show that doubling the temperature can lead to 120% increase of the bearing losses and up to 140% increase of the total transmission losses. The effect of the variation of operating conditions (velocity and torque) is also taken into account.

The novelty of this paper lays in the development of a dynamic model which takes into account the performance of a complete gearbox under transient operating conditions, as well as the interaction among its main components and the ability to make changes on the influencing factors of transmission efficiency so that their effect on the complete gearbox efficiency can be tracked. This has not been yet reported in the relevant literature which mainly focuses on the influencing factors of transmission power loss and efficiency experimental measurements under various operating conditions for gear pairs instead of complete gearboxes.

Keywords: Manual Transmission Model, Tapered Roller Bearing, Thermally Induced Preload, Frictional Losses

1. Introduction

The necessity for reduced fuel consumption and emissions due to the imposed regulations leads to the requirement for higher efficiency transmissions **[1]**. Nevertheless, in-depth research on the total frictional losses of gearboxes is not common in the available literature due to the fact that their efficiency is already considered high with values up to 97% **[2]**. Moreover, in the past years the main focus has been on controlling Noise, Vibration and Harshness (NVH).

However, research has been reported on the efficiency of manual transmissions. To be more precise, experimental measurements have been conducted by various researchers to track either the transmission power loss under various operating conditions or the effect of several factors on transmission efficiency **[3]**.

Nevertheless, due to the experimental nature of this research approach the influencing factors of gearbox efficiency are often summarized to the types of gears used in gearboxes or even the type of transmission, as well as the type of vehicle itself **[4]**. Another approach on estimating transmission efficiency has been the categorization of the different types of loses that occur both on the gears and the bearings of manual transmissions. Experimental tests have been conducted in order for this categorization as well as the proposed most dominant loss sources to be verified **[5, 6]**. However, this is not considered an approach for complete transmission efficiency since neither the interactions within the gear pairs nor between the gears and bearings is taken into consideration. On the other hand, literature findings show that transmission efficiency simulations are limited, especially when the effect of multiple influencing factors is taken into account or the interactions among the transmission main components **[7, 8]**. To be more precise, in most cases of calculating power losses, gear pairs or bearings are individually examined **[9]**. It should be mentioned that some approaches on the interaction between gears and bearings on the same shaft have been conducted but not for complete gearbox scale **[10]**. Nevertheless, predictions of complete transmission losses can be found in the literature. The models employed in most cases are quasi-static instead of dynamic and, most importantly, the interactions between the bearings and gear pairs are not taken into account even for cases that bearing losses are considered part of the total transmission efficiency calculation **[11].** To be more precise, on some cases, models have been developed in order to calculate specific types of losses even including experimental validation but usually they refer to a single gear pair, leading to misinterpretations of their effect on complete transmissions **[12].** It should be mentioned, however, that there are cases where a complete gearbox is examined but the operating conditions are not representative of a real automotive transmission (high speeds and torque values are not examined, the transient changes in the operating conditions cannot be tracked or there are difficulties on utilizing the low speed conditions **[13, 14].**

For the development of a complete automotive gearbox dynamic model, it is necessary to evaluate the power loss of its main components. Synchronizers and seals contribute to transmission losses; however, it has been shown **[15]** that their power losses 15% or less of the total transmission power loss and, consequently, may be neglected due to the fact that any improvements could not increase the total efficiency considerably. On the other hand, the efficiency of gears can vary based on the type employed with some types being highly efficient, reaching efficiency values of even 98%. Nevertheless, there are gear types characterized by 90% efficiency, which points to the need of investigating gear teeth mechanical losses **[16]**. Additionally, bearings are also used in every manual transmission and introduce frictional losses which make them the second most power consuming gearbox part **[17]**. Since tapered roller bearings are widely used in manual transmissions, it is important to study their performance and introduce improvements that could reduce their frictional losses. The effect of temperature on the performance of tapered roller bearings should also be taken into account since it vastly affects the value of thermally induced preload **[18]**.

The main types of bearing losses are due to viscous and boundary friction in the contacting elements **[19]**. For cylindrical roller bearings and tapered roller bearings the value of the initial preload can be an important factor for the generated friction during operation and even if it is carefully considered in the design stage it will always affect the power consumption **[20]**. Besides the initially applied preload, thermally induced preload is

also generated during operation due to uneven thermal expansion of the bearing components and has a consequence on bearing losses. Its effect can be reduced with preload compensation via different suggested mechanisms **[21]**.

The generation of thermally induced preload is completed in four stages: a) the heat generation due to friction, b) the heat transfer on the bearing parts, c) the component expansion following the heat transfer and d) the contact force induction **[22]**. The factors affecting the generated thermally induced preload are the bearing deflection caused by the instantaneous radial and axial forces, the uneven thermal expansion between the rollers, the outer ring / housing geometry and finally, the rotational speed of the bearing **[21]**. The thermally induced preload affects the efficiency of the complete transmission.

In this paper, a tribodynamic model of a manual transmission has been developed for calculating efficiency. The novelty of the model lies on the fact that it takes into account the interactions between the main gearbox components (gears and bearings) on calculating their mechanical losses leading to the prediction of the complete transmission system efficiency as well as the effect of temperature. Consequently, thermally induced preload is also considered. The simulations use the RDE driving cycle as input operating conditions to provide a useful predictive tool of the manual transmission losses for industry purposes. Results show that the temperature increase has a major effect on the generated frictional losses of the bearings (consequently adding to the total transmission losses).

2. Methodology

2.1 System Model Description

The manual transmission system model predicts the dynamics of gears and their effect on the tribological performance, hence efficiency of the tapered roller bearings. The simulations run for different temperatures of the bearing rolling elements in order to capture the temperature effect on preload and, consequently, on the friction generated at the bearings. The transmission examined is shown in figure 1.

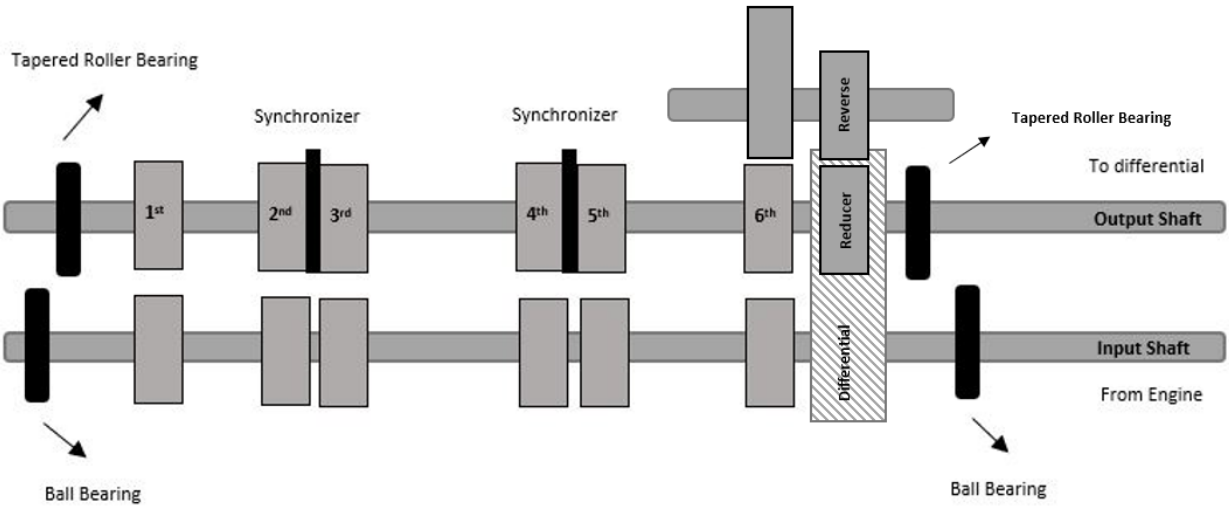

Figure 1 *The examined transmission layout*

In order for the model to calculate the complete frictional losses of a manual transmission, taking into account the interactions between gears and bearings, is of high importance. This is achieved by calculating the generated dynamic load during gear meshing and transferring its effect to the bearings. It has to be emphasized that the bearing loss calculations are not conducted simultaneously with gear meshing calculations **[23]**. Nevertheless, this approach can be reliable, since all the gear meshing data are used to evaluate the bearing condition. It should be pointed out that gear teeth modifications are not investigated in this research. The transmission was examined without assessing if different materials or geometry would have a beneficial effect on its efficiency.

The input shaft velocity values for each time step are taken from the RDE driving cycle. Based on the driving cycle data, the engaged gear is identified. For each gear pair (loaded or unloaded) the equations of motion are solved using an iterative method in Matlab. The equation of motion of each gear is solved using Matlab's ode45 function, which applies a Runge - Kutta iterative method to calculate the output shaft velocity for the loaded gear case (and that of the loose gear in the unloaded cases) and the loads on the gear teeth, with the different types of friction included.

It should be stressed that different equations of motions describe the operation of loaded and unloaded gears. The model has 6 rotational degrees of freedom due to the examined gearbox consisting of six gear pairs. One degree of freedom describes the dynamics of the engaged gear pair whereas the other five represent the loose gears. The simultaneous solution of the 6 DoF system of equations allows for calculating the transmission power loss at each instant of time. For the scenarios examined in this research either the first or the second gear pair is engaged. A similar approach (equations of motion) would be used for any other gear pair engaged, since the model created has the ability to track the engaged gear pair and modify its equation of motion. The following equations of motion are solved for the first gear pair being engaged **[24]**:

$$
\begin{aligned}
I_1 * \ddot{\theta}_1 &= T_1 + T_{d,1} - T_f - T_{g,viscous} - T_{g,boundary} \\
I_2 * \ddot{\theta}_2 &= T_{Wh,2} - T_{Ff,2} - T_{Fp,2} \\
I_3 * \ddot{\theta}_3 &= T_{Wh,3} - T_{Ff,3} - T_{Fp,3} \\
I_4 * \ddot{\theta}_4 &= T_{Wh,4} - T_{Ff,4} - T_{Fp,4} \\
I_5 * \ddot{\theta}_5 &= T_{Wh,5} - T_{Ff,5} - T_{Fp,5} \\
I_6 * \ddot{\theta}_6 &= T_{Wh,6} - T_{Ff,6} - T_{Fp,6}
\end{aligned} \tag{1}
$$

Where T_1 is the torque due to the engaged gear meshing, T_{Wh} is the torque due to the unloaded gear meshing, $T_{d,1}$ is the torque due to the engaged gear damping, T_f is the resisting torque, $T_{g,viscous}$ is the torque due to the viscous friction generated on the engaged gear, $T_{g,boundary}$ is the torque due to the boundary friction generated on the engaged gear, $T_{Ff,2}$ is the torque due to the flank friction generated on the unloaded gear, $T_{Fp,2}$ is the torque due to the generated friction between the unloaded gear and the shaft. Indices 1 to 6 refer to the six gears (speeds in rad/s) in the examined manual transmission **[25]**.

Consequently, for the case of the second gear pair being engaged, the set of equations of motion is modified to:

$$
\begin{aligned}
I_1 * \ddot{\theta}_1 &= T_{Wh,1} - T_{Ff,1} - T_{Fp,1} \\
I_2 * \ddot{\theta}_2 &= T_2 + T_{d,2} - T_f - T_{g,viscous} - T_{g,boundary} \\
I_3 * \ddot{\theta}_3 &= T_{Wh,3} - T_{Ff,3} - T_{Fp,3} \\
I_4 * \ddot{\theta}_4 &= T_{Wh,4} - T_{Ff,4} - T_{Fp,4} \\
I_5 * \ddot{\theta}_5 &= T_{Wh,5} - T_{Ff,5} - T_{Fp,5} \\
I_6 * \ddot{\theta}_6 &= T_{Wh,6} - T_{Ff,6} - T_{Fp,6}
\end{aligned} \tag{2}
$$

By solving the aforementioned set of equations of motion, the different reactions applied on gear pairs have been calculated. In order for the power losses to be calculated at each time step of operation, equation (3) is used which is modified based on the gear pair that is engaged. The power loss expression below assumes that the first gear pair is engaged:

$$
Power\ Loss = \left[\left(T_{f,1} + T_{g,viscous,1} + T_{g,boundary,1}\right) + \sum_{i=2}^{6}\left(T_{Ff,i} - T_{Fp,i}\right)\right]n \tag{3}
$$

where n is the speed of the shaft in rpm. Based on the loads that apply on gear teeth during meshing, the load applied on the tapered roller bearings is calculated. This load is then used to find the friction generated on the bearings. For each simulation a specific temperature value for the bearing rolling elements is assumed. Using this input, the corresponding thermally induced preload is calculated and used for calculating frictional losses. More details on the calculation of thermally induced preload and how it affects the friction calculations will

be provided in the following sections. A flowchart of the aforementioned methodology is presented in Appendix 2.

2.2 Applied Load on Tapered Roller Bearings and the Effect of Thermally Induced Preload

The main characteristic of tapered roller bearings is the ability to undertake both axial and radial loads **[4]**. For the current case of manual transmission, these loads are a result of gear meshing. However, in this section focus will be given on the calculation of the applied load on the bearing rolling elements since it is a complex procedure requiring an iterative method.

The application of load leads to two different deflections on the tapered roller bearing elements, one on axial (δ_α) and one on radial direction (δ_r) **[20, 26, 27]**:

$$\delta_\alpha = \left(\frac{F_\alpha}{zK_n J_a \sin(\alpha)}\right)^{0,9} + P_{r,ia} \tag{4}$$

$$\delta_r = \left(\frac{F_r}{zK_n J_r}\right)^{0,9} + P_{r,ir} \tag{5}$$

where F_α is the axial load applied on the tapered roller bearing, F_r is the radial applied load, z is the number of rolling elements, K_n is the load deflection factor, α is the contact angle of the bearing, $P_{r,ia}$ is the deflection caused due to initially applied preload on axial direction and $P_{r,ir}$ is the deflection caused due to initially applied preload on radial direction. The preload is usually considered to be applied in axial direction. However, due to the nature of tapered roller bearings a radial component is present, which is calculated as:

$$P_{r,ir} = P_{r,ia} \cos a \tag{6}$$

J_a and J_r are the axial and radial integrals, respectively. The values of these integrals depend on the load distribution factor e **[28]**:

$$e = \frac{1}{2}\left(1 + \frac{\delta_\alpha \tan(\alpha)}{\delta_r}\right) \tag{7}$$

Complicate differential equations describe the relationship between the integrals and the load distribution factors **[29].** However, solving these equations is not required since tables can be found in the literature, which describe their relationship via pre-calculation of these integrals. In this model, the aforementioned tables are used for connecting the value of both integrals with the load distribution factor. Even with the use of tables, an iterative method cannot be avoided. At each time step for the specific values of loads that are applied on both directions, the axial and radial deflections are calculated. The next step is the calculation of the load distribution factor. The integrals for the corresponding factor are traced by the tables used. The steps are repeated, and the

final values of the deflections are found. Appendix 3 presents a flowchart describing the method for the bearing load calculation.

As already mentioned, due to heat generation during bearing operation, an additional deflection due to thermally induced preload is built. This highly depends on the temperature that the gearbox is operating, as shown in equation (8) **[30]**, which is the reason for simulating different temperature conditions:

$$P_{r,Tr} = a_{th}(T - 20)r \tag{8}$$

Where $P_{r,Tr}$ is the deflection due to thermally induced preload of the bearing rolling element, inner or outer ring with respect to room temperature (20ºC), most commonly applied on the radial direction; a_{th} is the thermal expansion coefficient of the rolling element, inner or outer ring which depends on its material; T is the temperature of the rolling element, inner or outer ring and r is the rolling element, inner or outer ring radius. This equation is derived respect to room temperature (20ºC) which is also design reference temperature of the current transmission. This is now added to the text after equation (8) for clarification. It has to be highlighted that for this research project the expansion of the tapered roller bearing rolling element, inner or outer ring is considered while the axial thermal expansion of the shaft is ignored. However, for the bearing rolling element, inner or outer ring the expansion in both directions are investigated. Equation (8) should be implemented for all bearing components, the rolling elements and the inner and outer ring. The total value of deflection is given by:

$$P_{r,Ttotalr} = P_{r,Trollingr} + \frac{P_{r,Tinnerr} - P_{r,Touterr}}{2} \tag{9}$$

The thermal expansion preload, although defined for each element is assumed to be symmetric circumferentially neglecting manufacturing imperfections. Hence, it is also added to the overall preload which contributes to the overall deformations of equations (4) and (5). The total value of deflection is then calculated as:

$$P_{r,totalr} = P_{r,Tr} + P_{r,i}r \tag{10}$$

However, an axial component of thermally induced preload should be calculated as:

$$P_{r,totala} = P_{r,totalr} \sin a \tag{11}$$

After calculating the thermally induced preload, it is necessary for each time step of simulation to add its value on the bearing deflections as follows so that it is taken into account when calculating friction [**26**]:

$$\delta_\alpha = \left(\frac{F_\alpha}{zK_n J_a \sin\alpha}\right)^{0,9} + P_{r,totala} \tag{12}$$

$$\delta_r = \left(\frac{F_r}{zK_n J_r}\right)^{0,9} + P_{r,totalr} \tag{13}$$

By using the aforementioned equations for the deflection and the iterative method as described, the values of the axial and radial integrals are calculated. With these given, the calculation of the maximum value of the load applied on the normal direction on the bearing at each instant of time can be calculated as **[23]**:

$$q = \frac{F_r}{J_r z \cos(\alpha)} = \frac{F_\alpha}{J_\alpha z \sin(\alpha)} \tag{14}$$

This value of the total load is used for the calculation of the generated friction on the bearing rolling elements as will be described in the following sections. Equation (14) shows that the total applied load can be found either by using data for the axial or the radial directions. This is due to the fact that the contact angle of all the rolling elements of the tapered roller bearing is the same. It should be pointed out though that for the calculation of the integrals both the effect of axial and radial deflection has been taken into consideration.

The value of the maximum load as described in equation (14) is not evenly distributed around the bearing (as shown in figure 2). Consequently, it is necessary for each time step to track the value of load q_j which is actually applied on each rolling element of the bearing and is a function of its position around the shaft:

$$q_j = q\left[1 - \frac{1}{2e}(1 - \cos\psi)\right]^{10/9} \tag{15}$$

where ψ is the angle as indicated in figure 2. For each rolling element, an initial position around the shaft is considered and using the aforementioned equation and the change of angle ψ the load q_j at each instant of time is calculated.

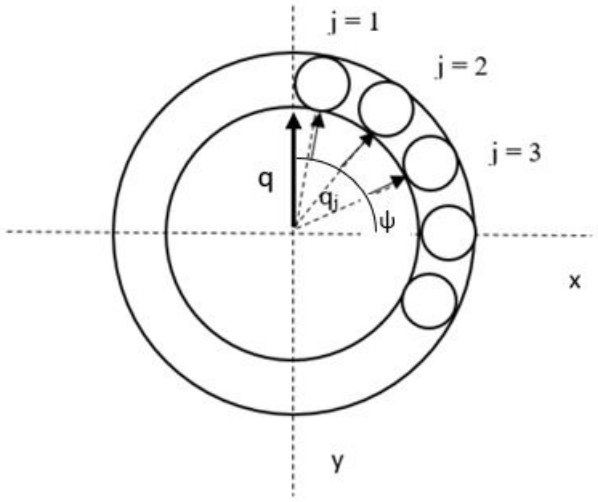

Figure 2 *Angle affecting load on bearing rolling elements*

2.3 Bearing Friction

The tapered roller bearings suffer mainly two types of friction, viscous and boundary, under elastohydrodynamic regime of lubrication due to the high speeds and loads under which the gearbox of a manual transmission operates **[31]**, whereas the rib contacts are not considered within this research. For the calculation of viscous friction at each instant, equation (16) is used **[32]**:

$$F_{viscous} = \mu q_j \tag{16}$$

where μ is the coefficient of friction and q_j is the applied load at each roller (at each instant of operation) that depends on the input applied load on the bearing and the angular position of each rolling element around the shaft. The coefficient of friction is given by **[33]:**

$$\mu = 0.87\alpha\tau_0 + 1.74\ \frac{\tau_0}{P_{mean}}\ \ln\left(\frac{1.2}{\tau_0 h_{c0}}\left(\frac{2\acute{K}\eta_0}{1+9.6\xi_j}\right)^{1/2}\right) \tag{17}$$

where α is the pressure-viscosity coefficient, h_{c0} is the dimensionless central film thickness, K is the conductivity of the lubricant, η_0 is the lubricant dynamic viscosity at atmospheric pressure and ξ is given by:

$$\xi_j = \frac{4}{\pi}\frac{K}{hc0/R_{x,j}}\left(\frac{P_{mean}}{E'R_x K\prime\rho\prime c\prime u_{r,j}}\right) \tag{18}$$

where R_x is the radii of curvature, K', ρ', c' are the thermal conductivity, density and specific heat capacity of the contacting solids and $u_{r,j}$ is the rolling velocity of the bearing rolling element **[34]**. The film thickness of the lubricant during operation, is given by:

$$h_{c0} = 4.31\left(\frac{\pi\eta_0 U}{4E_r R_x}\right)^{0.68}\left(\frac{2}{\pi}(E_r\alpha)\right)^{0.49}\left(\frac{\pi q}{2E_r {R_x}^2}\right)^{-0.073}\left\{1 - exp\left[-1.23\left(\frac{R_y}{R_x}\right)^{2/3}\right]\right\} \quad (19)$$

R_x, R_y are the radii of curvature along x and y direction, respectively, since an elliptical contact is considered **[35]** and E_r is the reduced elastic modulus of contact:

$$E_r = \frac{\pi}{((1-{\nu_1}^2)/E_1)+((1-{\nu_2}^2)/E_2)} \quad (20)$$

where ν_1, ν_2 is the Poisson ratio of the two contacting surfaces respectively, and E_1, E_2 is their Young's moduli of elasticity. U is the speed of lubricant given by:

$$U = \frac{u_i+u_{r,j}}{2} \quad (21)$$

where u_i is the surface velocity of the inner raceway.

The methodology for estimating boundary friction is then required for completing the calculation of total bearing frictional losses. In the case of tapered roller bearing used in transmission applications boundary friction applies due to the fact that thin lubricant films are present and asperity contact occurs. The method assumes a Gaussian height distribution of surface asperities. The formula for calculating boundary friction is given by:

$$F_{boundary} = \tau_L A_a \quad (22)$$

where, τ_L is the limiting shear stress and A_a is the asperity contact area **[36]**. The limiting shear stress is used, since the bearings perform under high pressures and thin films. As the sliding velocity increases the shear stress reaches the limiting value **[37]**. The limiting shear stress is given by:

$$\tau_L = \tau_0 + \varepsilon P_{mean} \quad (23)$$

where τ_0 is the Eyring stress, ε is the slope of the lubricant limiting shear stress-pressure curve and P_{mean} is the mean pressure applied on each roller at each instant of time during operation **[38]**, as described by:

$$P_{mean} = \frac{W_a}{A_a} \quad (24)$$

The Gaussian distribution of asperity peaks leads to a fraction of load that can be carried by these asperities **[39]**, as given by:

$$W_a = \frac{16\sqrt{2}}{15} * \pi * (\xi * \beta_a * \sigma)^2 * \sqrt{\frac{\sigma}{\beta_a}} * E' * A * F_{\frac{5}{2}}(\lambda) \quad (25)$$

In equation (24), ξ is the asperity density per unit area, β_a is the average asperity tip radius, σ is the composite

RMS surface parameter, A is the apparent contact area, E is the reduced elastic modulus of contact, as described in equation (27), and $F_{5/2}(\lambda)$ is a statistical function for a Gaussian distribution of asperities, as given in the following equation.

$$F_{5/2} = \begin{cases} -0.004\lambda^5 - 0.06\lambda^4 - 0.3\lambda^3, \lambda < 2.5 \\ -0.8\lambda^2 - 0.8\lambda - 0.6 \quad , \lambda < 2.5 \\ 0 \quad , \lambda \geq 2.5 \end{cases} \tag{26}$$

$$E' = {}^{2E_r}/_{\pi} \tag{27}$$

The asperity contact area A_α is described by:

$$A_a = \pi^2 * (\xi * \beta * \sigma)^2 * F_2(\lambda) \tag{28}$$

where $F_2(\lambda)$ is another statistical function for Gaussian distribution of asperities:

$$F_{5/2} = \begin{cases} -0.002\lambda^5 - 0.03\lambda^4 - 0.2\lambda^3, \lambda < 2.5 \\ +0.5\lambda^2 - 0.8\lambda - 0.5 \quad , \lambda < 2.5 \\ 0 \quad , \lambda \geq 2.5 \end{cases} \tag{29}$$

2.4 Unloaded Gear Modeling and Frictional Losses

Prior to calculating the gear teeth frictional losses, it is necessary to describe their meshing so that the loads and velocities applied on gears and transferred to bearings can be calculated. Additionally, it is necessary to separate the meshing modelling between loaded and unloaded gears since different conditions apply and their physics are not described by the same equations. In this section, the modelling of unloaded gears is described. The geometry of the gears examined plays crucial role on the calculation of their kinematics and consequently dynamics. In this case, helical gears are considered.

Based on the dimensions of the gear teeth, it is necessary to calculate the line of action. This way it is possible to track the number of teeth that are in contact simultaneously in relation with the total angular displacement of the gear. The number of teeth in mesh is necessary for the calculation of the oil film thickness that is concentrated on the gear teeth and of the load and friction that are generated during operation. The line of action is described by **[40]**:

$$L_{act} = \sqrt{FW^2 + {Z_{act}}^2} \tag{30}$$

where FW is the gear face width and Z_{act} is the length of action on the transverse plane of the helical gear.

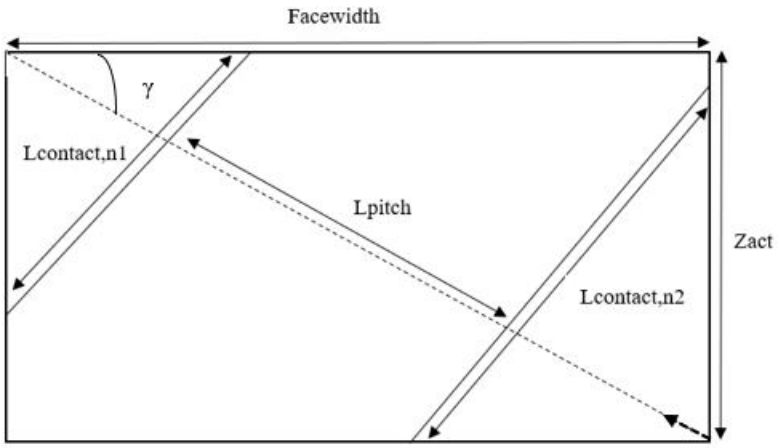

Figure 3 *Helical Gear Teeth Contact Path*

Within the model, the number of teeth (n) that are simultaneously in contact is captured. For each tooth that is in mesh at the specific time step examined, it is necessary to calculate the contact length, shown as $L_{contact}$ in figure 3. It should be pointed out that n_1 and n_2 in the same figure refer to tooth 1 and 2 being in contact simultaneously. The equation for calculating the contact length is given by:

$$L_{contact,n1} = R_{pw} \sin a_p - \sqrt{{R_{ow}}^2 - {R_{bw}}^2} - \left[\left(\frac{\theta_p R_{bp} \cos\beta}{\sin(\beta+\gamma)}\right)(I-N)L_{pitch} \sin\gamma\right] \quad (31)$$

where R_{pw} is the wheel pitch radius, a_p is the pressure angle, R_{ow} is the wheel outer radius, R_{bw} is the wheel base radius, θ_p is the pinion angular displacement, R_{bp} is the pinion base radius, β is the helix angle, γ is the angle shown in figure 3, L_{pitch} is the diagonal pitch along the line of action, N is the number of teeth in contact and I = 1,…., N. For the rest of the calculations it is also required to find the equivalent radius of curvature. In order to achieve that, for each gear pair, the instantaneous contact radius of the wheel and the pinion are calculated as:

$$r_w = \frac{\sqrt{R_{ow}^2 - R_{bw}^2} - \varphi_p R_{bp}}{\cos\beta} \quad (32)$$

$$r_p = \frac{C_c \sin a_t}{\cos\beta} - r_w \quad (33)$$

where R_{ow} and R_{bw} are the outer and base radii of the wheel of the contacting gear pair respectively, R_{bp} is the base radius of the pinion, φ_p is the angle describing the position of each contact point, β is the helix angle, a_t is the transverse pressure angle and C_c is the gear pair centre distance. Finally, the equivalent radius of curvature is defined as shown in equation (34). It has to be noted that the radius of curvature is calculated at each time instant in the dynamic model and is constantly changing.

$$r_{eq} = \frac{r_p r_w}{(r_p + r_w)\cos\beta} \quad (34)$$

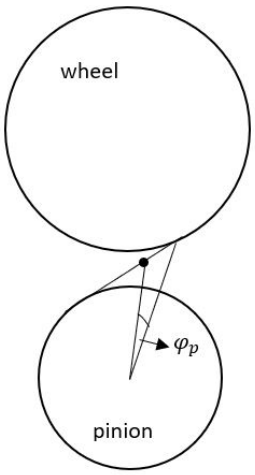

Figure 4 Position of contact point in angular terms

It should be pointed out that for helical type of gears the theoretical contact line is considered a straight line and the lubricant entrainment direction is the direction that defines the transverse plane, which results to not having any curvature on y direction **[41].**

The unloaded gear teeth are under hydrodynamic regime of lubrication. The film thickness in the normal section is given by **[42]**:

$$h = \begin{cases} C_b - \frac{R_{bp}\varphi_p - R_{bw}\varphi_w}{\cos a_t}, & R_{bp}\varphi_p > R_{bw}\varphi_w \\ C_b, & R_{bp}\varphi_p = R_{bw}\varphi_w \\ C_b + \frac{R_{bp}\varphi_p - R_{bw}\varphi_w}{\cos a_t}, & R_{bp}\varphi_p < R_{bw}\varphi_w \end{cases} \quad (35)$$

where C_b is the half backlash value and φ_p, φ_w are the angular displacement of the pinion and the wheel, respectively. The squeeze velocity with first order approximation is given by:

$$\frac{\partial h}{\partial t} = \begin{cases} -\frac{R_{bp}\dot{\varphi}_p - R_{bw}\dot{\varphi}_w}{\cos a_t}, & R_{bp}\varphi_p > R_{bw}\varphi_w \\ 0, & R_{bp}\varphi_p = R_{bw}\varphi_w \\ \frac{R_{bp}\dot{\varphi}_p - R_{bw}\dot{\varphi}_w}{\cos a_t}, & R_{bp}\varphi_p < R_{bw}\varphi_w \end{cases} \quad (36)$$

The lubricant reaction on the gear teeth was calculated for hydrodynamic regime of lubrication which is considered applicable due to the low loads of unengaged teeth **[43]**:

$$W_h = \begin{cases} \frac{L_{contact}\eta_0 r_{eq}}{h}\left(2u - \frac{3\pi}{\sqrt{\frac{2h}{r_{eq}}}}\frac{\partial h}{\partial t}\right), & \frac{\partial h}{\partial t} < 0 \\ \frac{L_{contact}\eta_0 r_{eq}}{h}(2u), & \frac{\partial h}{\partial t} \geq 0 \end{cases} \quad (37)$$

The first type of friction generated on the gear teeth is viscous friction, which for the case of gears is usually referred as flank friction **[44]**. The hydrodynamic viscous friction is described by:

$$\mathrm{F_f} = \begin{cases} \frac{\mathrm{L}_{contact}\pi\eta_0\Delta\mathrm{u}}{\sqrt{2\mathrm{h}}}\sqrt{\mathrm{r_{eq}}} & ,\Delta\mathrm{u} \geq 0 \\ \frac{\mathrm{L}_{contact}\pi\eta_0(-\Delta\mathrm{u})}{\sqrt{2\mathrm{h}}}\sqrt{\mathrm{r_{eq}}} & ,\Delta\mathrm{u} < 0 \end{cases} \tag{38}$$

Where Δu is the sliding velocity calculated for each time step. For the unloaded gear case, no boundary friction is generated since the applied loads are not high enough to lead to interaction of asperities. The second type of losses on unloaded gears is the journal bearing friction generated between the shaft and the gear (frequently called as Petrov friction). It is given by:

$$F_p = \frac{2\pi\eta_0 u R_{bw} l_{rg}}{C_c} \tag{39}$$

where l_{rg} is the gear flank width **[45]**.

2.5 Loaded Gear Modelling and Frictional Losses

In order for the model to track the effect of bearing thermally induced preload on the total power losses, the prediction of the loaded gear pair dynamics is necessary. Even though gear kinematics can be defined as described in the previous section for the unloaded gears, the load and friction of the gear teeth are given by different equations since the hydrodynamic regime of lubrication no longer applies. Elastohydrodynamic lubrication regime is considered instead. The load that applies on the engaged teeth during the meshing as a result of the gear stiffness is given by:

$$W = \begin{cases} k\left(R_{bp}\varphi_p - R_{bw}\varphi_w\right) - C_b\,, & DTE > C_b \\ 0 & ,\ |DTE| < C_b \\ k\left(R_{bp}\varphi_p - R_{bw}\varphi_w\right) + C_b & ,\ DTE < -C_b \end{cases} \tag{40}$$

where k is the meshing stiffness and DTE is the dynamic transmission error **[46]**. The meshing stiffness k is calculated using British Standard ISO 6336. It is necessary first to calculate the stiffness k_{tooth} of a single tooth pair, which is given by the following formula:

$$k_{tooth} = C_M k_{th} C_R C_B \cos\beta \tag{41}$$

where C_M is the correction factor equal to 0.8 for solid gears, k_{th} is the theoretical single stiffness, C_R is the gear blank factor (1 for solid gears), C_B is the basic rack factor and β is the helix factor. The theoretical single stiffness is given by the following equation:

$$k_{th} = \frac{1}{q'} \tag{42}$$

$$\text{with } q' = 0.04723 + {}^{0.15551}\Big/_{\left(z_p/\cos^3\beta\right)} + {}^{0.25791}\Big/_{\left(z_w/\cos^3\beta\right)}. \tag{43}$$

where z_p, z_w are the number of teeth of the pinion and the wheel respectively and x_1, x_2 are the addendum modification coefficients of the pinion and the wheel. The basic rack factor is calculated as:

$$C_B = \left[1 + 0.5\left(1.2 - h_{fp}/m_n\right)\right]\left[1 - 0.02\left(20 - a_p\right)\right] \tag{44}$$

where h_{fp} is the dedendum of the basic rack of cylindrical gears, m_n is the gear module and a_p is the pressure angle. Then, the total stiffness is given by:

$$k = L_{contact}\, k_{tooth} \tag{45}$$

where $L_{contact}$ is the total length of the contact lines, which is also affected by the number of teeth that are in contact simultaneously during the meshing.

The teeth of loaded gears transfer high torques leading to the generation of both viscous and boundary friction under elastohydrodynamic regime of lubrication. For helical gears, the contact line is considered straight so the contact that will be used for the calculation of friction is line contact and the curvature is calculated only for the major axis of the entraining motion of the lubricant. For calculating friction a similar method to that applied on bearings is used. The viscous friction is given by:

$$F_{g,viscous} = \mu_g W \tag{46}$$

where μ_g is the coefficient of friction which is calculated as described for the bearing case in equation (17) **[41]**.

The high loads that apply on the engaged gear teeth lead to the generation of boundary friction in addition to viscous friction. The methodology followed for the calculation of boundary friction is similar with that described for the tapered roller bearings:

$$F_{g,boundary} = \tau_{g,L}\, A_{g,a} \tag{47}$$

where $\tau_{g,L}$ is the limiting shear stress and $A_{g,a}$ is the asperity contact area **[47]**, as given in equations (23) - (28) for the bearing case. However, gear data are used this time and line contact is considered.

2.5 Churning Losses

Finally, for completing the calculation of gearbox losses and its efficiency, churning losses should also be considered as described below for dip lubrication conditions used in the examined gearbox.

$$P_{VZ0} = T_H \frac{\pi n}{30} \tag{48}$$

where $T_{H,i}$ is the total hydraulic loss torque and n is the rotational speed **[48].** The total hydraulic loss torque is calculated as:

$$T_H = C_{Sp} C_1 e^{C_2\left(\frac{v_t}{v_{t0}}\right)} \tag{49}$$

where C_{Sp} is the splash oil factor and $C_{1,2}$ state the effect of the tooth width and the immersion depth. They are described by the following set of functions:

$$\left.\begin{aligned} C_{Sp} &= \left(\frac{4h_{e,max}}{3h_c}\right)^{1.5} \frac{2h_c}{l_h} \\ C_1 &= 0.063\left(\frac{h_{e1}+h_{e2}}{h_{e0}}\right) + 0.0128\left(\frac{b}{b_0}\right)^3 \\ C_2 &= \frac{h_{e1}h_{e2}}{80h_{e0}} + 0.2 \end{aligned}\right\} \tag{50}$$

where $h_{e,max}$ is the maximum tip circle immersion depth with stationary oil level, h_c is the height of the point of contact above the lowest point of the immersing gear, l_h is the hydraulic length, $h_{e1,e2}$ are the tip circle immersion depth with stationary oil level, h_{e0} is the reference value of the immersion depth, b is the tooth width and b_0 is the reference value of the tooth width **[49]**.

3. Results

3.1 Experimental Measurements

In order for the transmission model to use realistic data, the gear and bearing element surface properties are experimentally measured using the Alicona Infinite Focus Measurement Machine (IFM). This allows for more direct comparison against the transmission experimental measurements. This device is used to obtain the surface properties of an examined object by identifying the height differences within its points by scanning the surface from its lowest to its highest point. The resolution under which the scanning process is conducted can be as low as 20nm. Appropriate software allows for the surface recreation with its main features **[50].**

In Table 1, the distribution of asperities for both bearings and gears (first gear) are presented as captured experimentally. Additionally, the surface properties are also provided. The gears and bearings used for the experimental measurements came from a used gearbox for a passenger car. This specific gearbox has only been

used for additional experimental measurements. The measurement data for all gears and bearings were used in the simulations for calculating friction of each one of them.

Table 1 *a) Distribution of Asperities for the Roller of the Tapered Roller Bearing, b) Height Parameters for the Roller of the Tapered Roller Bearing, c) Distribution of Asperities of the First Gear, d) Height Parameters of First Gear.*

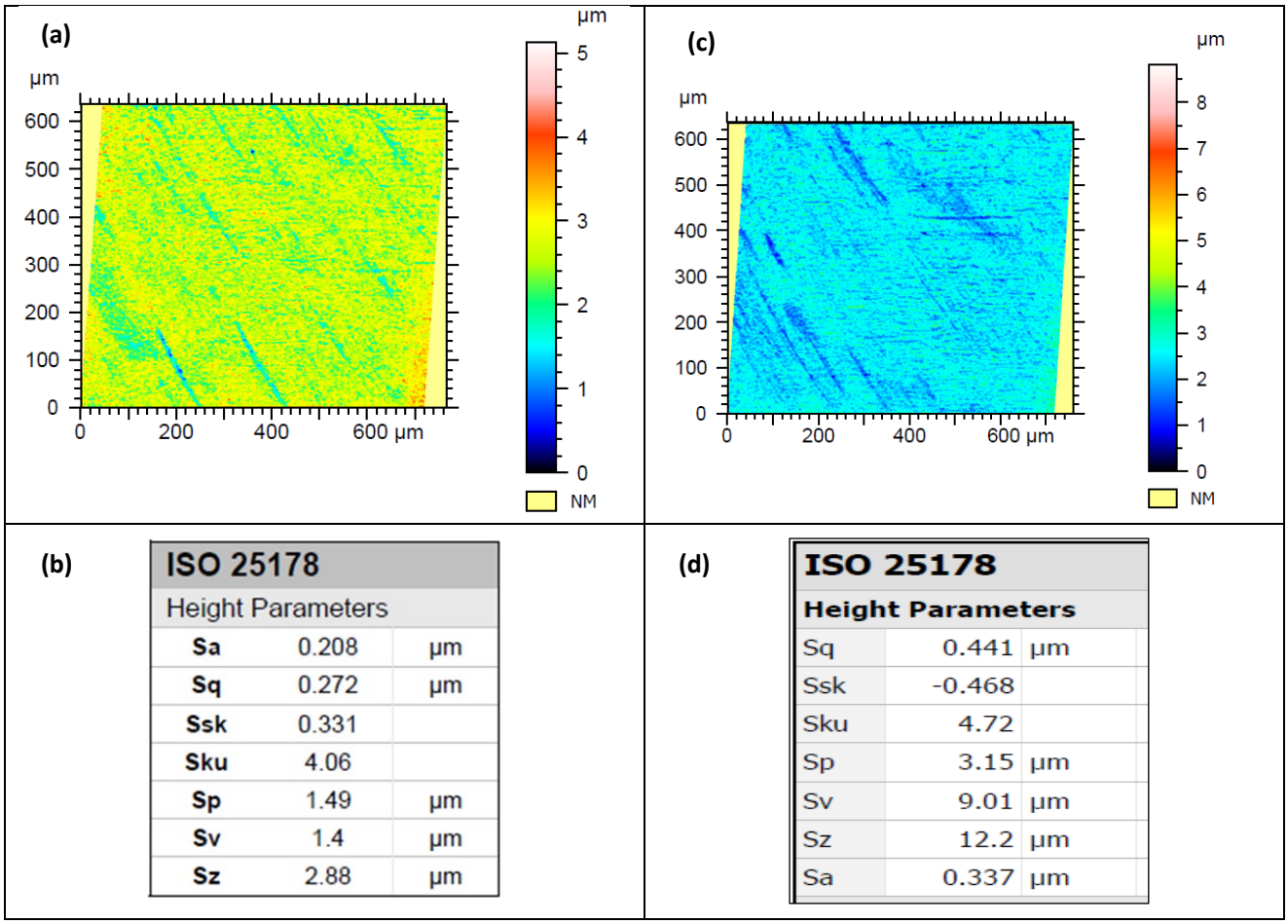

(b)

ISO 25178		
Height Parameters		
Sa	0.208	µm
Sq	0.272	µm
Ssk	0.331	
Sku	4.06	
Sp	1.49	µm
Sv	1.4	µm
Sz	2.88	µm

(d)

ISO 25178		
Height Parameters		
Sq	0.441	µm
Ssk	-0.468	
Sku	4.72	
Sp	3.15	µm
Sv	9.01	µm
Sz	12.2	µm
Sa	0.337	µm

It should be highlighted that within the different gears the surface properties can differ significantly, up to 20%. however, this is due to the fact that is designed to be engaged in severely different operating conditions. It should also be pointed out that for the bearing surface measurements a fit to plane options was used during the postprocessing of the data so that the round shape of the rolling elements would not affect the height of asperities that was captured.

3.2 Model Validation

The 6-speed manual transmission employed in this project is used in small to medium passenger cars. The gear data are shown in Table 2.

Table 2 *Gear data*

Gear Speed		***Number of Teeth***	***Module***	***Pitch Radius [mm]***	***Pressure Angle [°]***	***Helix Angle [°]***	***Gear Width [mm]***	***Tip Diameter [mm]***	***Gear Ratio***
1	Pinion	12	2.12	56.39448995	21	29	11.5	35.2	1.1219
	Wheel	41	2.12	50.26465673	21	29	17.7	101.8	
2	Pinion	24	1.5915	45.38187	19.25	28.75	15	49	0.5319
	Wheel	47	1.5915	85.31792	19.25	28.75	16.3	87.77	
3	Pinion	29	1.7652	57.71158	18.5	27.5	15.2	62.63	0.7837
	Wheel	37	1.7652	73.63202	18.5	27.5	15.65	76.33	
4	Pinion	35	1.6	66.77234	17	33	14.9	71.79	1.0606
	Wheel	33	1.6	62.95678	17	33	15.75	67.76	
5	Pinion	37	1.67	73.67613	17	33	13.8	78.49	1.3214
	Wheel	28	1.67	55.75491	17	33	14.15	61.22	
6	Pinion	41	1.59754	41.43646116	17	31.5	14.6	82.37	1.7600
	Wheel	26	1.59754	23.54344202	17	31.5	15.95	55.31	

Additionally, the properties of the lubricant used are provided in Table 3. The temperature effect on lubricant dynamic viscosity has been taken into consideration. For the viscosity measurements, the lubricant was heated using a hot plate and a thermocouple captured the temperature. It has to be noted that the temperature corresponds to the lubricant sump. Then, with the use of a viscometer the dynamic viscosity was measured multiple times for consistency purposes.

Table 3 a) Lubricant Properties b) Dynamic viscosity for different temperatures

a)

Pressure viscosity coefficient [1/Pa]	$1.05*10^{-8}$
Lubricant conductivity [W/m*K]	0.137

b)

Temperature [ºC]	**Dynamic Viscosity [Pa s]**
20	0.055
40	0.042
80	0.030

The input conditions for model simulations are taken from the RDE driving cycle, which is presented in figure 5. It was decided to test two small parts of the cycle. The conditions of these parts are in detail described in table 4.

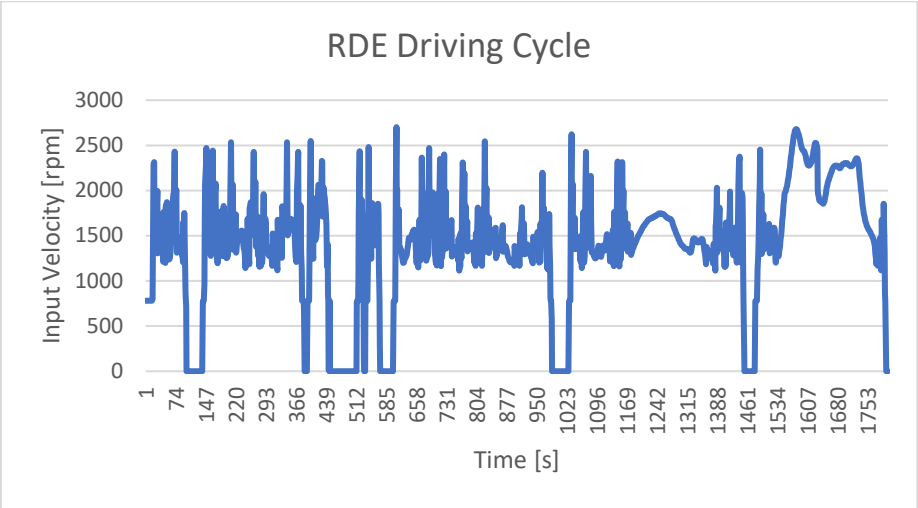

Figure 5 *RDE driving cycle*

The aforementioned model for calculating the complete transmission losses as a system requires validation in order to be applied for different case scenarios of operating conditions. Experimental data collected for the RDE cycle from a vehicle equipped with the same transmission show the power losses variation for several input velocity and torque combinations, as presented in figure 6. The experimental measurements of the gearbox power loss were conducted in a test rig comprising an electrically driven dynamometer, the examined transmission, thermocouples to trace oil temperature and torque meters. An oil cooling device keep the temperature stable. Each test runs for 20 minutes and the engagement of the gear pair is established prior the beginning of the test. The variation of the input shaft speed is maximum 3% of the set value whereas the same applies to the input torque as well. The temperature change for the experiment to be considered accurate should be ± 2^{o}C of the set temperature. The output torque measurement deviation is also around 3%.

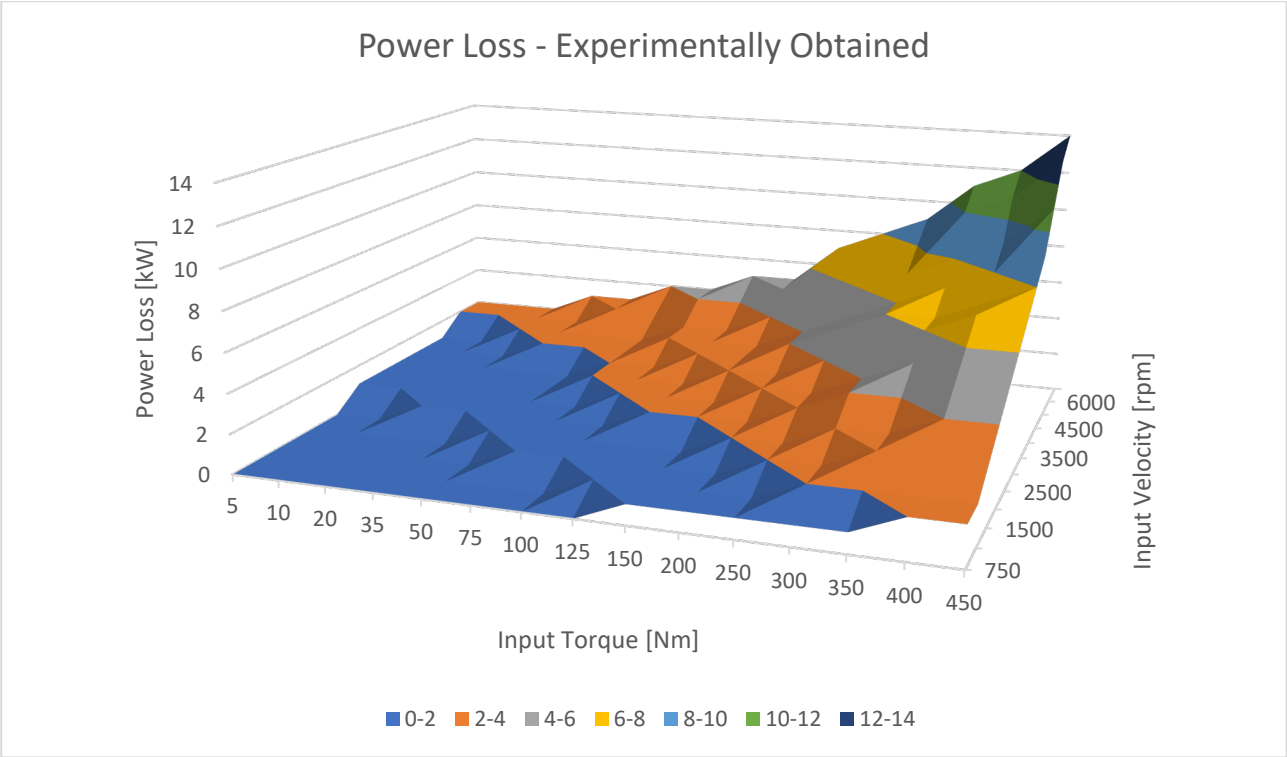

Figure 6 *Transmission Power Losses Obtained Experimentally*

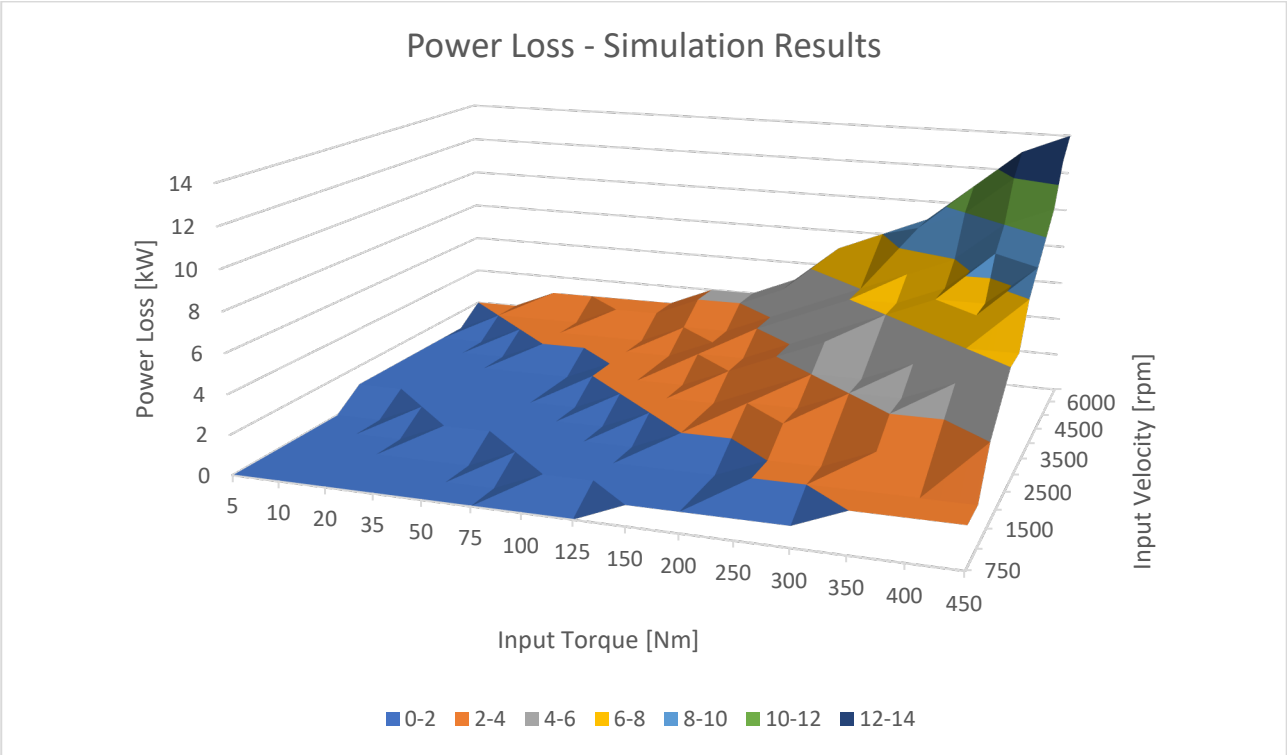

Figure 7 *Transmission Power Losses obtained from Simulations*

In order for the model to be evaluated it was decided to run simulations for the same input velocity - torque combinations and the results to be compared against the experimental data. The simulation results are presented in figure 7. It was observed that in the examined cases, the difference between the simulation results and the experimental data is less than 14%. This verifies that the model is a reliable tool to calculate the frictional

losses of a vehicle's manual transmission. The following table shows in more detail the power loss difference (percentage) between simulation results and experimental measurements for various operating conditions corresponding to the results of figures 6 and 7. Additionally, the values in parentheses in Table 5 have been calculated by taking into consideration the highest errors of the measurements. To be more precise, we have used +3% on both torque and speed data and recalculated the differences presented in Table 5 (for the most extreme values of the table) using the new input values. As it can be seen, the additional percentage difference is no more than 1.5% even when considering the highest measurement errors.

Table 4 *Difference (percentage %) between power loss simulation results and experimental measurements. Values in parentheses represent the difference for the experimentally obtained data with the errors taken into account*

		Input speed [rpm]				
		1000	**2000**	**3000**	**4000**	**5000**
Input torque [Nm]	**10**	-1.25	11.00 (12.48)	2.69	3.77	-1.46
	50	6.59	4.65	6.00	3.97	-2.78
	100	-8.57	-9.34 (-10.56)	-4.22	0.80	-2.53
	200	-7.71	-13.91 (-13.85)	-7.03	-4.96	-2.51
	300	-3.22	-7.58	-2.09	-5.62	0.17
	400	1.28	-5.19	-2.61	0.32	-2.87

3.3 Simulation Results

The dynamic model previously described was used for various parts of the RDE driving cycle (and different temperature values for the rolling elements of the tapered roller bearings in order to include the effect of thermally induced preload) to calculate the frictional losses of the complete transmission in comparison with the temperature variation during operation. In this section, the results will be discussed.

Three scenarios were examined, as illustrated in table 4. For the first two scenarios the input velocity was considered the same and only a temperature rise is applied for assessing the effect of thermally induced preload. For the third scenario a different part of the RDE driving cycle was employed so that a different gear pair is engaged.

Table 4 *RDE Cycle Scenarios examined*

Scenario	***RDE Cycle Time Part [s]***	***Input Shaft Velocity Range [rad/s]***	***Input Torque [Nm]***	***Engaged Gear***	***Temperature [^{o}C]***
1	1 – 16	81 – 83	5	1	40
2	1 – 16	81 – 83	5	1	80
3	20 – 30	170 – 190	23	2	80

The different temperatures were mainly chosen to trace their effect on the thermally induced preload. The values chosen are representative of gearbox operating conditions and commonly used by automotive manufactures as a metric when comparing transmission efficiency. The value of the initially applied preload (deflection) is typically measured at 20ºC and for the simulations was assumed at $0.01 \cdot 10^{-5}$ m. For the first scenario the temperature was set to 40ºC. The value of thermally induced preload is $1.3405 \cdot 10^{-5}$ m and as a result the total preload is $1.3505 \cdot 10^{-5}$ m. When the temperature increases to 80ºC for the second scenario, the thermally induced preload changes to $2.6810 \cdot 10^{-5}$ m and the total to $2.6910 \cdot 10^{-5}$ m. The same preload value applies on the third scenario as well.

For the first scenario examined, the transmission power losses are presented in figure 8. The use of the dynamic model allows for calculating the complete gearbox losses. However, the amount of each different type that applies is also calculated. The combination of using RDE cycle parts and identifying the engaged gear paper as well as the use of original gear dimensions and surface properties makes the following results representative of the operation of the transmission in a realistic scenario. Results show that the churning losses of the gearbox followed by the frictional losses of the loaded gear. It should be highlighted that since the model takes into account the presence of all gears simultaneously the losses of the unloaded gears are presented as a whole. However, separate calculation is also possible since the friction of each gear, loaded or unloaded, is also approached individually. It is also important to mention that even though the effect of churning losses is quite high compared to the other frictional losses, the combined generated friction on the loaded gear is comparable to the churning loss value. The model has the ability to test the effect of changes on the gear properties, such the use of different materials or coating, or minor modifications on the geometry of the gear, and track the effect on each type of loss as well as the effect on efficiency.

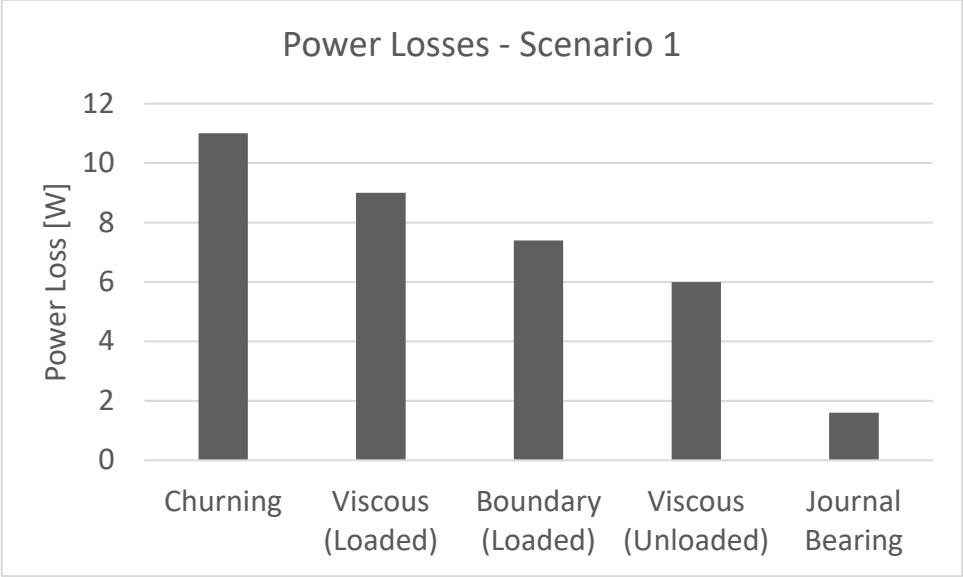

Figure 8 *Gear Losses for Scenario 1*

The power losses for the third scenario are shown in figure 9. It should be remined that the difference between scenarios 2 and 3 is the temperature change. Nevertheless, it was identified that when gears are only considered

for the power losses and not the bearings temperature does not have a major effect leading to a minor increase at the total power losses, less than 1%, which is the reason for presenting the losses for scenario 3 only.

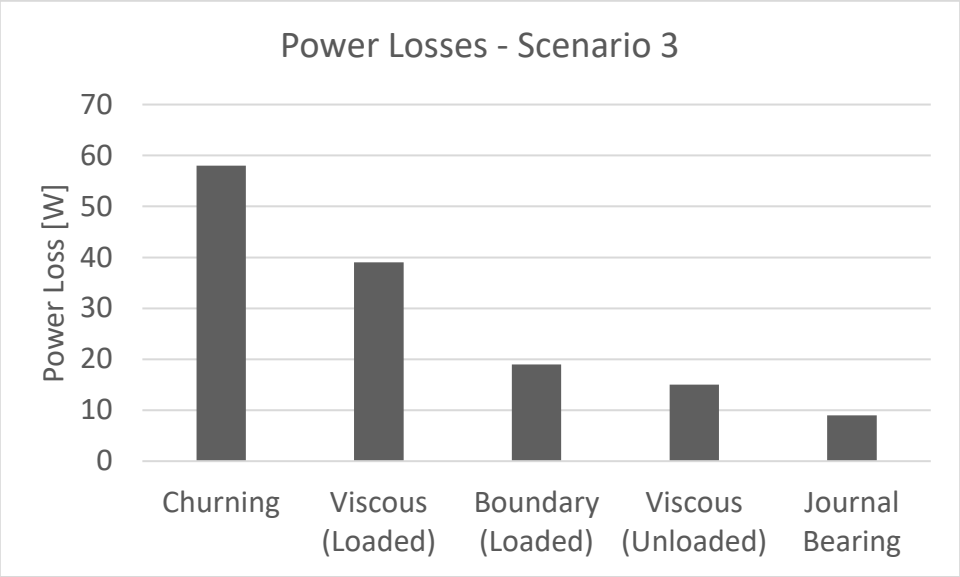

Figure 9 *Gear Losses for Scenario 3*

The losses calculated as presented in figure 9 show that the operating conditions of the transmission have a major effect on the generated losses. Since the change of the engaged gear is tracked within the model and the input conditions have been modified, it is obvious that a small but abrupt change during driving can lead to a major change on the transmission efficiency. Though, the apportionment within the types of losses follows the same pattern as described previously. For this case though, the ability of the model to interact with the gear characteristics is of high importance since the difference that could be achieve for increasing transmission efficiency could be higher and lead to complete transmission efficiency improvement since the values of the frictional losses are affected by the gear properties more than the churning losses.

Afterwards, the rolling element bearing losses for the three different scenarios examined are illustrated in figure 10. For the cases of the bearings, it is necessary to present all the examined cases since both the operating conditions and the temperature influence the values of the generated friction respectively. Even though the values are lower compared to those of gears, the effect of bearing losses cannot be neglected when calculating transmission efficiency. It has to be highlighted that even for the same operating conditions the temperature change can increase the power losses of bearings highly. For double the operating temperature, the total power losses of the bearing increase more than double for all the examined cases. Also, it should be reminded that the values of the generated friction are, among others, a result of the meshing forces that are generated at the same time on gears since the model created includes the interaction between the two main transmission components. Due to the fact that viscous friction is for all cases higher than boundary friction, it is very important when examining transmission efficiency to be able to interact with the surface properties of the components. Additionally, it should not be neglected that even though both the operating conditions as well as temperature have significant effects on the generated friction, the levels of importance are comparable.

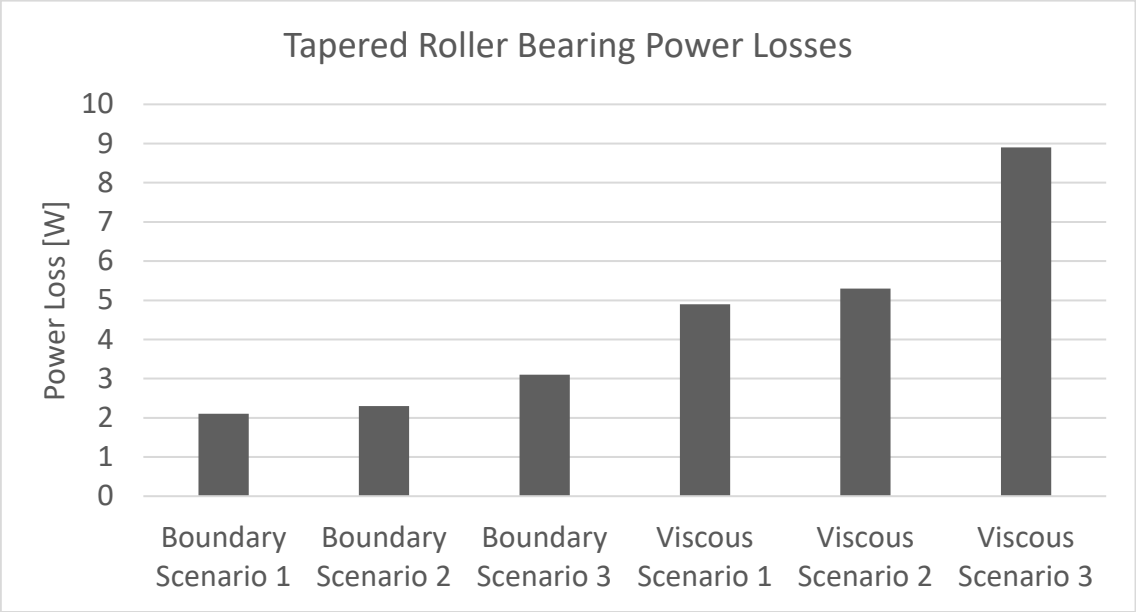

Figure 10 *Rolling Element Bearing Losses*

Figure 11 illustrates the bearing losses for the three scenarios examined, with the addition of two more scenarios in which the third and fourth gear are engaged with the gearbox operating at 1500 rpm and 45 Nm input torque. The temperature was assumed to be 80oC for both new scenarios. The percentage of power loss in tapered roller bearings was calculated using the following formula:

$$Loss_{b,p} = \frac{Bearing\ Power\ Loss\ [W]}{Total\ Power\ Loss\ [W]} 100 \tag{51}$$

The results in figure 11 show that bearings can play a key role on transmission efficiency. To be more precise, when the transmission is not operating under extreme torques, the bearing power consumption increases, especially when temperature is considered. It appears that the combination of high temperatures and low to moderate low toque values (scenarios 2-5) constitutes operating conditions where control of the temperature effect by thermally induced preload could improve the total transmission efficiency.

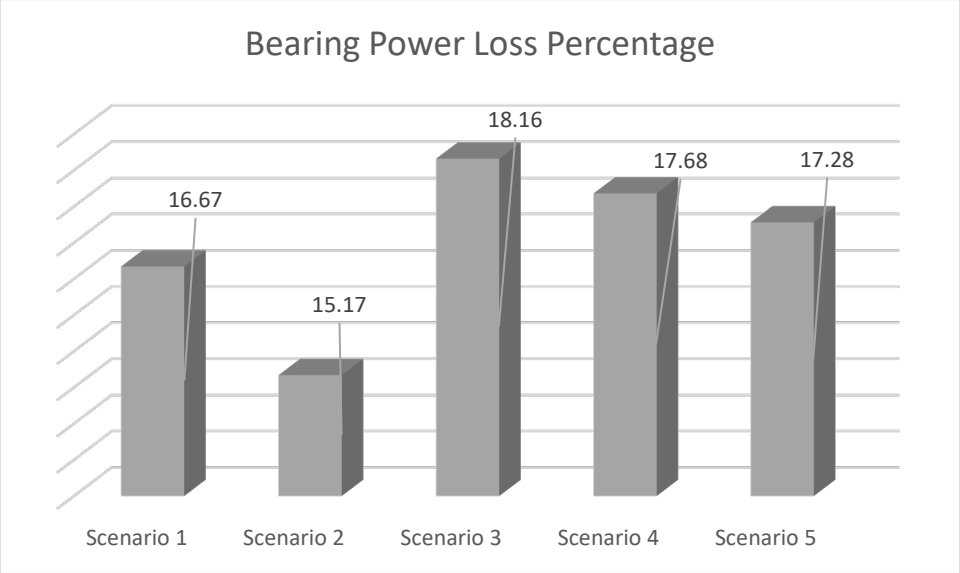

Figure 11 *Percentage of bearing losses compared to total transmission power loss for high temperatures.*

The findings of the simulation results are summarized in figure 12 where the effect of each power loss type on the total transmission losses is presented. The level of churning losses is really high when compared with each one of the other types of friction that appear during the transmission operation. However, the combined effect of the all the other types is obviously compared with that of churning losses and, subsequently, updates that could be conducted that reduce the values of the other losses can definitely increase complete transmission efficiency. The ability of the created model to easily modify various parameters, surface characteristics or geometry, could relatively conveniently help identify the factors that are more worthy of further research.

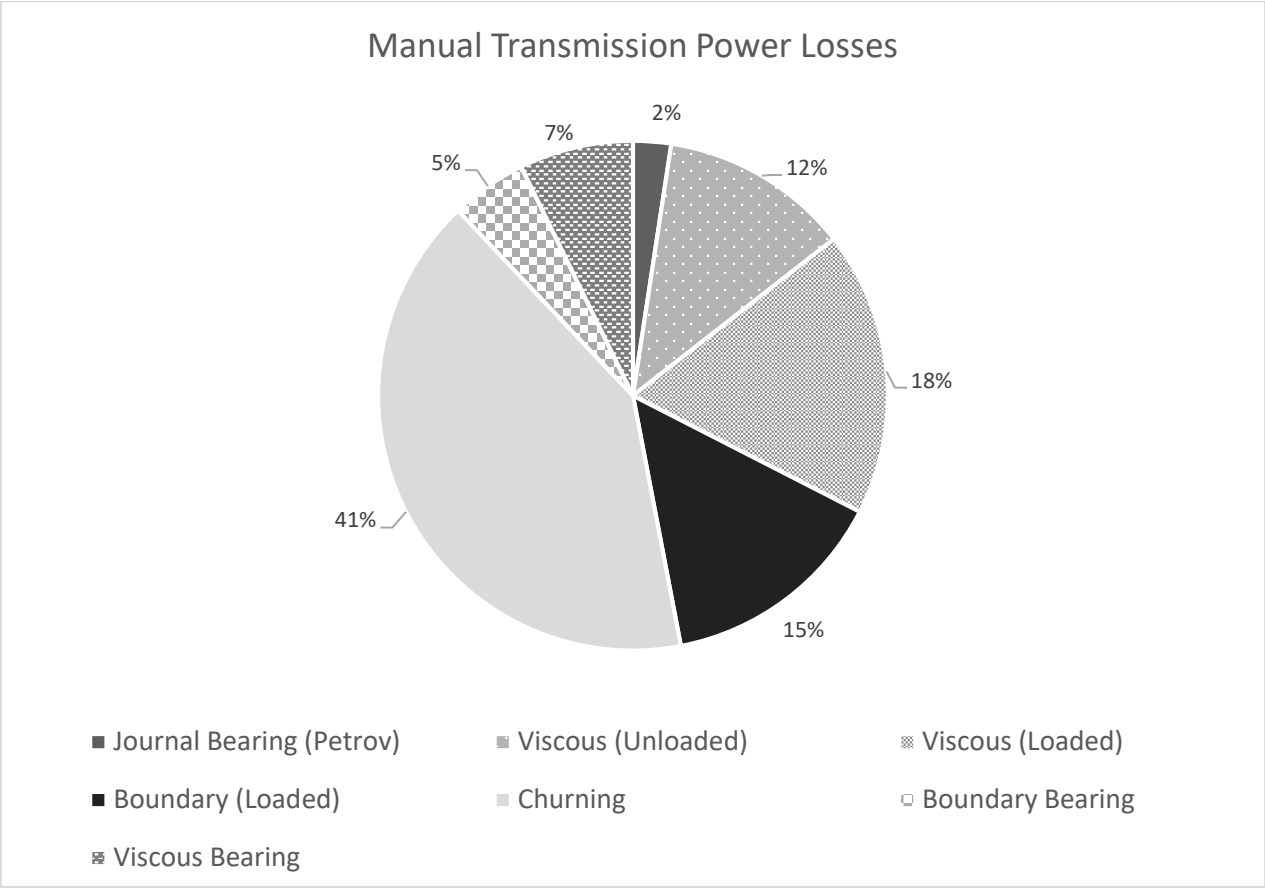

Figure 12 *Manual Transmission Power Losses*

4. Conclusion

In this paper, a transmission tribodynamic model has been developed that captures the load and friction generated due to gear meshing and bearings simultaneously. RDE driving cycle conditions were used as input so that the results are representative of realistic OEM transmission testing. The temperature effect on thermally induced preload and, as a result, bearing friction was taken into account, showcasing that the model is able to predict the changes in transmission efficiency. The power losses of the manual transmission were compared against experimentally obtained values, validating the model.

The amount of power loss both on bearings and gears lead to the conclusion that there is still room for improvement on each gearbox component that could lead to overall gearbox efficiency improvement. To be more precise, it was identified that churning losses have the most effect on total transmission losses representing around 40%. The next highest contribution originates from the viscous friction of the loaded gear (21% of the total power loss). Finally, the frictional (power) loss of the bearings was identified as an important factor for efficiency (14% of the total transmission losses) especially due to the dependence on temperature, which is a parameter not easy to control.

Additional investigation on the variation of bearing losses compared to total transmission losses was conducted in order to verify the importance of temperature. To be more precise, it was identified that the combination of

low input loads and high temperatures, which is part of the RDE driving cycle, can lead to huge increase of the bearing frictional losses compared to the other components, highlighting once again the importance of temperature control.

As part of the future work, it is the aim of the authors to include additional components (such as seals and synchronizers) in the study of transmission power loss, in order to provide a more complete picture. Additionally, the control of the temperature effect on power losses by considering thermally compensating bearings, is another future task.

Acknowledgment

The authors would like to express their gratitude to Ford Motor Company for its financial support under its University Research Programme.

References

1 **Tung, S.C. & McMillan, M.L.,** 2004. Automotive tribology overview of current advances and challenges for the future. Tribology International, 37(7), pp.517–536.

2 **Schaffner, T. et al.,** 2014. Investigating the efficiency of automotive manual gearboxes by experiment and simulation. Proceedings of the Institution of Mechanical Engineers, Part K: Journal of Multi-body Dynamics, 228(4), pp.341–354. Available at: http://pik.sagepub.com/lookup/doi/10.1177/1464419314539302.

3 **Joachim, J. & Börner, J.,** 2012. How to Minimize Power Losses in Transmissions , Axles and Steering Systems. Gear Technology, September(September), pp.58–66.

4 **Schlegel, C., Hösl, A. & Diel, S.,** 2009. Detailed Loss Modelling of Vehicle Gearboxes. *Proceedings 7th Modelica Conference*, pp.434–443. Available at: http://www.ep.liu.se/ecp_article/index.en.aspx?issue=043;article=48.

5 **Höhn, B. R., Michaelis, K., & Hinterstoißer, M.** ,2009. Optimization of gearbox efficiency. *Goriva i maziva*, *48*(4), 462.

6 **Michaelis, K., Höhn, B. R., & Hinterstoißer, M.** ,2011. Influence factors on gearbox power loss. Industrial lubrication and tribology, 63(1), 46-55.

7 **Fernandes, C.M.C.G. et al.,** 2014a. Gearbox power loss. Part I: Losses in rolling bearings. Tribology International, 88, pp.298–308. Available at: http://dx.doi.org/10.1016/j.triboint.2014.11.017.

8 **Fernandes, C.M.C.G. et al.,** 2014b. Gearbox power loss. Part II: Friction losses in gears. Tribology International, 88, pp.309–316. Available at: http://dx.doi.org/10.1016/j.triboint.2014.12.004.

9 **Joachim, F. J., Börner, J., & Kurz, N.**, 2014. Power losses in transmissions, axles, and steering systems. In Encyclopedia of Lubricants and Lubrication (pp. 1398-1411). Springer, Berlin, Heidelberg.

10 **Changenet, C., Oviedo-Marlot, X., & Velex, P.,** 2006. Power loss predictions in geared transmissions using thermal networks-applications to a six-speed manual gearbox. Journal of Mechanical Design, 128(3), 618-625.

11 **Heingartner, P., & Mba, D., 2003**, January. Determining power losses in helical gear mesh: Case study. In ASME 2003 International Design Engineering Technical Conferences and Computers and Information in Engineering Conference (pp. 965-970). American Society of Mechanical Engineers.

12 **Seetharaman, S. et al.,** 2009. Oil Churning Power Losses of a Gear Pair: Experiments and Model Validation. *Journal of Tribology*, 131(2), p.22202.

13 **Marques, P. M., Fernandes, C. M., Martins, R. C., & Seabra, J. H.,** 2013. Power losses at low speed in a gearbox lubricated with wind turbine gear oils with special focus on churning losses. *Tribology International*, *62*, 186-197.

14 **Bourdon, A., Rigal, J.F. & Play, D**., 1999. Static rolling bearing models in a CAD environment for the study of complex mechanisms: Part II – C.

15 **Andersson, M.,** 2014. Churning losses and efficiency in gearboxes (Doctoral dissertation, KTH Royal Institute of Technology).

16 **Petry-Johnson, T. T., Kahraman, A., Anderson, N. E., & Chase, D. R.,** 2008. An experimental investigation of spur gear efficiency. *Journal of Mechanical Design*, *130*(6), 062601.

17 **Carmichael, G. D. T., & Davies, P. B.,** 1970. Measurement of thermally induced preloads in bearings. *Strain*, *6*(4), 162-165.

18 **Gupta, P. K. ,** 1979. Dynamics of rolling-element bearings—part IV: Ball bearing results. Journal of lubrication technology, 101(3), 319-326.

19 **Ozturk, E., Kumar, U., Turner, S., & Schmitz, T.,** 2012. Investigation of spindle bearing preload on dynamics and stability limit in milling. *CIRP Annals-Manufacturing Technology*, *61*(1), 343-346.

20 **Takabi, J. & Khonsari, M.M.,** 2013. Experimental testing and thermal analysis of ball bearings. *Tribology International*, 60, pp.93–103. Available at: http://dx.doi.org/10.1016/j.triboint.2012.10.009.

21 **Stein, J.L. & Tu, J.F.,** 1994. A State-Space Model for Monitoring Thermally Induced Preload in Anti-Friction Spindle Bearings of High-Speed Machine Tools. *Journal of Dynamic Systems, Measurement, and Control*, 116(3), pp.372–386.

22 **Weck, M., McKeown, P., Bonse, R., & Herbst, U. ,**1995. Reduction and compensation of thermal errors in machine tools. *CIRP Annals-Manufacturing Technology*, *44*(2), 589-598.

23 **Mohammadpour, M., Theodossiades, S., & Rahnejat, H. ,**2014. Multiphysics investigations on the dynamics of differential hypoid gears. Journal of Vibration and Acoustics, 136(4), 041007.

24 **DelaCruz, M.A.** ,2011, The influence of transient thermo - elastohydrodynamic conjuctions on automotive transmission rattle (Doctoral Disserattion).

25 **Mohammadpour, M., Theodossiades, S., & Rahnejat, H.,** 2014. Transient mixed non-Newtonian thermo-elastohydrodynamics of vehicle differential hypoid gears with starved partial counter-flow inlet boundary. Proceedings of the Institution of Mechanical Engineers, Part J: Journal of Engineering Tribology, 228(10), 1159-1173.

26 **Harris, T. A. ,**1971. The endurance of a thrust-loaded, double row radial cylindrical roller bearing. *Wear*, *18*(6), 429-438.

27 **Jorgensen, B.R. and Shin, Y.C.,** 1997. Dynamics of machine tool spindle/bearing systems under thermal growth. *TRANSACTIONS-AMERICAN SOCIETY OF MECHANICAL ENGINEERS JOURNAL OF TRIBOLOGY*, *119*, pp.875-882.

28 **Demirhan, N., & Kanber, B.,** 2008. Stress and displacement distributions on cylindrical roller bearing rings using FEM. *Mechanics Based Design of Structures and Machines*, *36*(1), 86-102.

29 **Harris, T. A. ,** 2001. Rolling bearing analysis. John Wiley and sons.

30 **Jorgensen, B.R. and Shin, Y.C.,** 1997. Dynamics of machine tool spindle/bearing systems under thermal growth. *TRANSACTIONS-AMERICAN SOCIETY OF MECHANICAL ENGINEERS JOURNAL OF TRIBOLOGY*, *119*, pp.875-882.

31 **Takabi, J., & Khonsari, M. M.,** 2016. On the thermally-induced failure of rolling element bearings. Tribology International, 94, 661-674.

32 **Johnson, K. L., & Greenwood, J. A.,** 1980. Thermal analysis of an Eyring fluid in elastohydrodynamic traction. *Wear*, *61*(2), 353-374.

33 **Evans C.R. and Johnson K.L.,** Regimes of traction in elastohydrodynamic lubrication, Proc Instn Mech Engrs, 200(C5): 313- 324, 1986.

34 **Chittenden RJ, Dowson D, Dunn JF, et al**. A theoretical analysis of the isothermal elastohydrodynamic lubrication of concentrated contacts. II. General case, with lubricant entrainment along either principal axis of the Hertzian contact ellipse or at some intermediate angle. Proc Roy Soc Ser A 1985; 397: 271–294.

35 **Mohammadpour, M., Rahmani, R. and Rahnejat, H.,** Effect of cylinder deactivation on the tribo-dynamics and acoustic emission of overlay big end bearings, Proceedings of the Institution of Mechanical Engineers, Part K: Journal of Multibody Dynamics. 2014, 228(2): 138-151

36 **Johnson, K. L., & Greenwood, J. A.,** 1980. Thermal analysis of an Eyring fluid in elastohydrodynamic traction. *Wear*, *61*(2), 353-374.

37 **Johnson, K. L., & Cameron, R.,** 1967. Fourth paper: shear behaviour of elastohydrodynamic oil films at high rolling contact pressures. *Proceedings of the Institution of Mechanical Engineers*, *182*(1), 307-330.

38 **Briscoe BJ, Evans DC.** The shear properties of Langmuir-Blodgett layers. InProceedings of the Royal Society of London A: Mathematical, Physical and Engineering Sciences 1982, 380(1), No. 1779, pp. 389-407.

39 **Greenwood J.A., and Tripp J.H.,** The contact of two nominally flat rough surfaces, Proc Instn Mech Engrs 185: 625-633, 1970.

40 **De la Cruz, M., 2010.** The influence of transient thermo-elastohydrodynamic conjunctions on automotive transmission rattle. Loughborough University, Loughborough, UK.

41 **Xu, H., Kahraman, A., Anderson, N. E., & Maddock, D. G.,** 2007. Prediction of mechanical efficiency of parallel-axis gear pairs. *Journal of Mechanical Design*, *129*(1), 58-68.

42 **Theodossiades, S., Tangasawi, O., & Rahnejat, H.**, 2007. Gear teeth impacts in hydrodynamic conjunctions promoting idle gear rattle. *Journal of sound and vibration*, *303*(3-5), 632-658.

43 **De la Cruz, M., Theodossiades, S., & Rahnejat, H.,** 2010. An investigation of manual transmission drive rattle. *Proceedings of the Institution of Mechanical Engineers, Part K: Journal of Multi-body Dynamics*, *224*(2), 167-181.

44 **Tangasawi, O., Theodossiades, S., & Rahnejat, H.,** 2007. Lightly loaded lubricated impacts: idle gear rattle. *Journal of Sound and Vibration*, *308*(3-5), 418-430.

45 **De la Cruz, M., Theodossiades, S., & Rahnejat, H.,** 2010. An investigation of manual transmission drive rattle. *Proceedings of the Institution of Mechanical Engineers, Part K: Journal of Multi-body Dynamics*, *224*(2), 167-181.

46 **Theodossiades, S., & Natsiavas, S.** ,2000. Non-linear dynamics of gear-pair systems with periodic stiffness and backlash. *Journal of Sound and vibration*, *229*(2), 287-310.

47 E**lisaus, V., Mohammadpour, M., Theodossiades, S., & Rahnejat, H.,** 2017. Effect of teeth micro-geometrical form modification on contact kinematics and efficiency of high performance transmissions. *Proceedings of the Institution of Mechanical Engineers, Part K: Journal of Multi-body Dynamics*, *231*(3), 538-555.

48 **Changenet, C., & Velex, P.,** 2008. Housing influence on churning losses in geared transmissions. *Journal of Mechanical Design*, *130*(6), 062603.

49 **LePrince, G., Changenet, C., Ville, F., Velex, P., Dufau, C., & Jarnias, F.** ,2011. Influence of aerated lubricants on gear churning losses–an engineering model. *Tribology Transactions*, *54*(6), 929-938.

50 **Schroettner, H., Schmied, M., & Scherer, S.** ,2006. Comparison of 3D surface reconstruction data from certified depth standards obtained by SEM and an infinite focus measurement machine (IFM). *Microchimica Acta*, *155*(1-2), 279-284.

APPENDIX 1

Notation

a	pressure-viscosity coefficient
A	apparent contact area
A_a	bearing asperity contact area
$A_{g,a}$	gear asperity contact area
b	tooth width
b_0	reference value of tooth width
c	damping coefficient
c'	specific heat capacity of solid
$C_{1,2}$	factors of tooth width and immersion depth
C_b	gear pair half backlash
C_B	basic rack factor
C_c	gear pair center distance
C_M	stiffness correction factor
C_R	gear blank factor
C_{Sp}	splash oil factor
DTE	dynamic transmission error
E	reduced elastic modulus of contact
e	load distribution factor
E_r	reduced elastic modulus of contact
F_α	axial load on bearing
F_f	hydrodynamic flank friction force
F_r	radial load on bearing
$F_{boundary}$	bearing boundary friction
$F_{g,boundary}$	gear boundary friction
$F_{viscous}$	bearing viscous friction
$F_{g,viscous}$	gear viscous friction
$F_2(\lambda)$	statistical function for a Gaussian distribution of asperities
$F_{5/2}(\lambda)$	statistical function for a Gaussian distribution of asperities
h	film thickness
h_c	height of contact above the lowest point of the immersing gear
h_{c0}	dimensionless central film thickness
$h_{e1,e2}$	tip circle immersion depth with stationary oil level
$h_{e,max}$	maximum tip circle immersion depth with stationary oil level
h_{e0}	reference value of the immersion depth
h_{fp}	dedendum of basic rack of cylindrical gears
I_i	ith gear stiffness
J_a	axial integral
J_r	radial integral
k	Stiffness
k_{th}	theoretical single stiffness
k_{tooth}	single tooth stiffness
K	conductivity of the lubricant

K'	solid thermal conductivity
K_n	load deflection factor
L_{act}	line of action
$L_{contact,n1}$	contact length
l_h	hydraulic length
l_j	distance between instantaneous point of contact and pitch point
L_{pitch}	pitch line
l_{rg}	gear flank width
m_n	gear module
n	rotational speed
n_i	number of tooth pair in contact simultaneously
P_b	base pitch
P_{mean}	mean pressure
P_p	circular pitch
$P_{r,ia}$	initially applied preload on axial direction
$P_{r,ir}$	initially applied preload on radial direction
$P_{r,Tinnerr}$	thermally induced preload of bearing inner ring
$P_{r,Touterr}$	thermally induced preload of bearing outer ring
$P_{r,Tr}$	thermally induced preload on radial direction
$P_{r,Trollingr}$	thermally induced preload of bearing rolling element
$P_{r,totala}$	total preload on axial direction
$P_{r,totalr}$	total preload on radial direction
$P_{r,Ttotalr}$	thermally induced preload
P_{VZ0}	churning losses
q	maximum applied load on bearing
q_j	rolling element load
r	bearing component radius
R_{bp}	pinion base radius
R_{bw}	wheel base radius
r_{eq}	equivalent radius of curvature
r_p	pinion instantaneous contact radius
R_{pp}	pinion pitch radius
R_{pw}	wheel pitch radius
r_w	wheel instantaneous contact radius
R_{op}	pinion outer radius
R_{ow}	wheel outer radius
R_x	radii of curvature along x direction
R_y	radii of curvature along y direction
T	temperature of bearing component
T_i	ith loaded gear torque
$T_{d,i}$	Ith gear torque due to damping
T_f	Resisting torque
$T_{Ff,i}$	ith gear torque due to flank friction
$T_{g,boundary}$	ith the torque due to boundary friction
$T_{g,viscous}$	ith torque due to viscous friction

T_H	total hydraulic loss torque
$T_{Fp,i}$	ith gear torque due to Petrov friction
$T_{Wh,i}$	ith unloaded gear torque
U	speed of lubricant
u_{entr}	entraining speed
u_i	surface velocity of the inner raceway
$u_{r,j}$	rolling velocity of bearing rolling element
v_{pp}	pinion pitch velocity
v_{sp}	pinion surface speed
v_{sw}	wheel surface speed
v_{wp}	wheel pitch velocity
W	loaded gear contact load
W_a	fraction of load carried by asperities peaks
W_h	unloaded gear contact load
x_1	addendum modification coefficients of the pinion
x_2	addendum modification coefficients of the wheel
z	number of rolling elements of the bearing
z_p	number of teeth of the pinion
z_w	number of teeth of the wheel
α	bearing contact angle
a_p	Pressure angle
α_t	transverse pressure angle
a_{th}	thermal expansion coefficient
β	helix angle
β_a	average asperity tip radius
δ_α	axial deflection of bearing rolling elements
δ_r	radial deflection of bearing rolling elements
Δu	sliding speed
ε	slope of the lubricant limiting shear stress-pressure curve
η_0	dynamic viscosity of the lubricant at atmospheric pressure
$\ddot{\theta}_i$	ith gear rotational speed
∂h	squeeze velocity
μ	bearing coefficient of friction
μ_g	gear coefficient of friction
$\nu_{1,2}$	Poisson ratio of contacting surfaces
ξ	asperity density per unit area
ρ'	density of solid
σ	composite RMS surface parameter
τ_0	Eyring stress
$\tau_{g,L}$	gear limiting shear strees
τ_L	bearing limiting shear stress
φ_p	pinion angular displacement
$\dot{\varphi}_p$	pinion angular velocity
φ_w	wheel angular displacement
$\dot{\varphi}_w$	wheel angular velocity

APPENDIX 2

System Model Flowchart

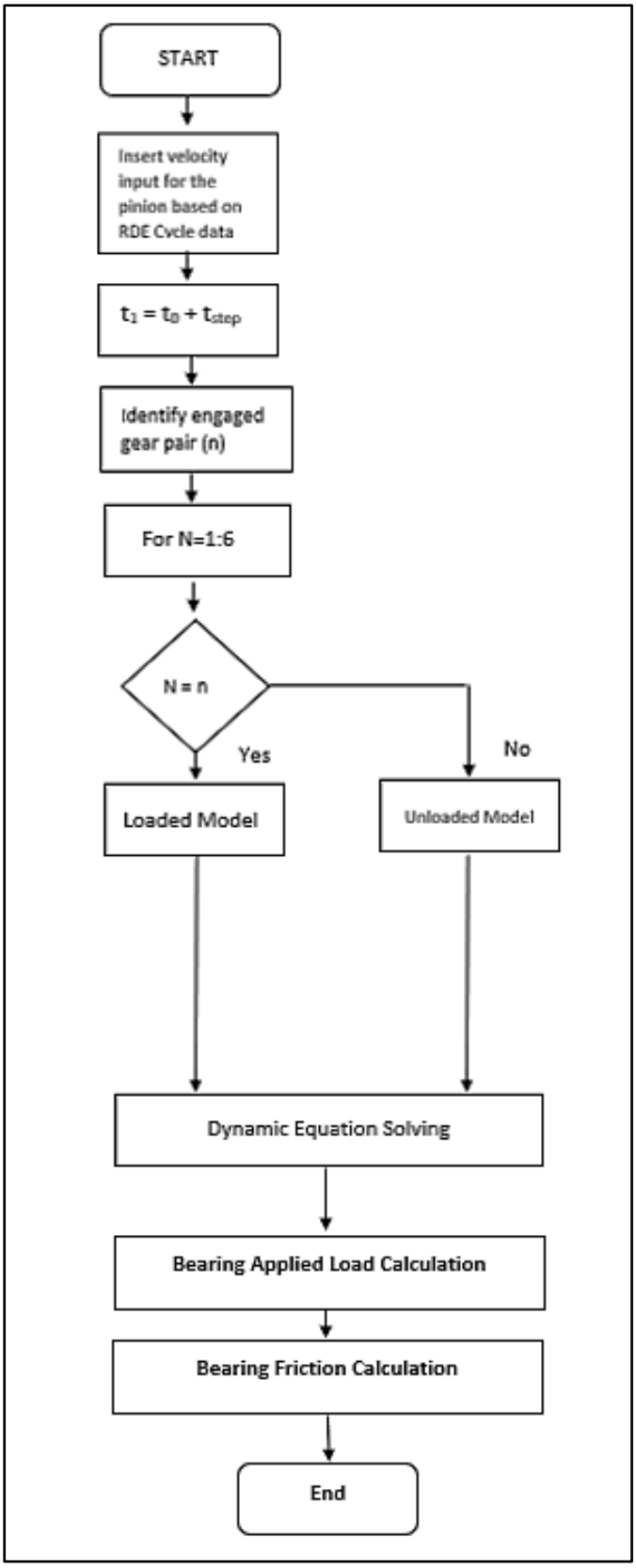

APPENDIX 3

Bearing Model Flowchart